Asian Summer Precipitation over the Past 544 Years Reconstructed by Merging Tree Rings and Historical Documentary Records

HUI SHI

Department of Atmospheric Sciences, School of Ocean and Earth Science and Technology, University of Hawaiʻi at Mānoa, Honolulu, Hawaii

BIN WANG

Department of Atmospheric Sciences, School of Ocean and Earth Science and Technology, University of Hawaiʻi at Mānoa, Honolulu, Hawaii, and Earth System Modeling Center, Nanjing University of Information Science and Technology, Nanjing, China

EDWARD R. COOK

Tree-Ring Laboratory, Lamont-Doherty Earth Observatory, Columbia University, Palisades, New York

JIAN LIU

Key Laboratory of Virtual Geographic Environment, Ministry of Education, School of Geography Science, Nanjing Normal University, Nanjing, China

FEI LIU

Earth System Modeling Center, and Climate Dynamics Research Center, Nanjing University of Information Science and Technology, Nanjing, China

ABSTRACT

Sparse long-term Asian monsoon (AM) records have limited our ability to understand and accurately model low-frequency AM variability. Here we present a gridded 544-yr (from 1470 to 2013) reconstructed Asian summer precipitation (RAP) dataset by weighted merging of two complementary proxies including 453 tree-ring-width chronologies and 71 historical documentary records. The RAP dataset provides substantially improved data quality when compared with single-proxy-type reconstructions. Skillful reconstructions are obtained in East and North China, northern India and Pakistan, the Indochina Peninsula, midlatitude Asia, the Maritime Continent, and southern Japan. The RAP faithfully illustrates large-scale regional rainfall variability but has more uncertainties in representing small-scale local rainfall anomalies. The RAP reproduces a realistic climatology and captures well the year-to-year rainfall variability averaged over monsoon Asia, arid central Asia, and all of Asia during the twentieth century. It also shows a general agreement with other proxies (speleothems and ice cores) during the period of 1470–1920. The RAP captures the remarkably abrupt change during the 1600s recorded in the upwelling proxy over the Arabian Sea. Four major modes of variability of the Asian summer precipitation are identified with the long record of the RAP, including a biennial El Niño–Southern Oscillation (ENSO) mode, a low-frequency ENSO mode, a central Pacific El Niño–like decadal mode, and an interdecadal mode. In sum, the RAP provides a valuable dataset for study of the large-scale Asian summer precipitation variability, especially the decadal–centennial variability that is caused by external forcing and internal feedback processes within the Earth climate system.

---

1. Introduction

The Asian monsoon (AM) region supports the livelihoods of about two-thirds of the world's humanity. Monsoon rainfall amount, variability, and associated climate extremes have been crucial to agricultural production and the welfare of the population for millennia. However, it remains a great challenge for models to accurately predict its seasonal anomalies (e.g., Wang et al. 2009). The year-to-year fluctuations of the monsoon rainfall are generally nonstationary over multidecadal to centennial time scales (e.g., Webster et al. 1998; Webster 2006). The causes of decadal–centennial variations of the Asian summer monsoon are not well understood (e.g., Goswami et al. 2006; Wang et al. 2018). Limited length of the instrumental data, which only dates back to a century or so, makes it difficult to investigate the interdecadal to centennial variability of the AM (Clemens 2006).

Multiple proxies, including ice cores, tree rings, speleothems, lake sediments, and historical documents, have been used to extend the monsoon climate records back in time at annual to decadal temporal resolution (Clemens 2006; P. Wang et al. 2005, 2014). But these climate reconstructions have been frequently restricted by the temporal resolution and spatial coverage of the proxies used, which only allows monsoon subsystems to be studied separately on regional scales (e.g., Zhu and Wang 2002; Zhang et al. 2003; Duan et al. 2004; Chen et al. 2011; Yi et al. 2012; Shi et al. 2014; Sinha et al. 2011, 2015; Xu et al. 2013, 2015; Gou et al. 2015; Tan et al. 2015). To assess the regional differences and their linkages to large-scale circulation, a well-calibrated, high-spatial-resolution reconstruction with full coverage of the Asian continental region is in great need.

Cook et al. (2010) presented the first gridded monsoon reconstruction, the Monsoon Asia Drought Atlas (MADA), for the past millennium based on a spatially extensive tree-ring network over the AM region. While the response of incremental tree growth to both soil moisture and temperature variation might be expected to parallel a drought severity index, the Palmer drought severity index (Dai et al. 2004) is not an ideal variable to pinpoint the dynamical processes and circulation patterns related to monsoon rainfall variability. It is also noted that the MADA performs poorly in reproducing dry/wet conditions in East China (Yang et al. 2013a; Yang et al. 2014; Zheng et al. 2014b; Ge et al. 2016; Kang et al. 2014), likely because of the tree-ring-data void in this region (Fig. 1a).

An invaluable resource recording past monsoon variability in East China is the dryness/wetness index. Although the sources of these indices vary (e.g.,

Chinese Academy of Meteorological Science China Meteorological Administration 1981; Zhang 1983; Wang and Zhao 1979), they are all derived from local chronicles across China since 1470 and/or the 500-yr flood/drought atlas, and are considered to reflect the changes in the East Asian monsoon rainfall. These indices, combined with other proxies, for example, tree rings, ice cores, and long-term instrumental measurements, have been used to reconstruct the past boreal warm-season (May–September) precipitation for the Asian continent (Feng et al. 2013; Shi et al. 2017). One of the issues related to such reconstructions, and also discussed in previous studies, is that the documentary data are temporally inhomogeneous. Depending on the availability of the instrumental data at each station, the dryness/wetness index could be derived exclusively from observed precipitation data (Zhang and Liu 1993). This is especially the case for the stations that have relatively long records, whose indices after 1950 are derived from observation alone (Wang et al. 2000). This means that the calibration using the data for the 1950–99 period is essentially inadequate. In addition, Feng et al. (2013) incorporated long-term instrumental records from India and South Korea, which might make the reconstruction spatially inhomogeneous.

In this study, we initiated multiple efforts to produce a new long-term monsoon record contributing to the AM reconstruction endeavor. First, we used only tree-ring data and historical documentary records in the reconstruction; no individual long instrumental records and other sparsely distributed proxy data were directly used to maintain the homogeneity of the reconstruction. Second, compared with the previous tree-ring network (Cook et al. 2010), a more comprehensive tree-ring dataset was used with additional 126 chronologies (Cook 2015; Cook et al. 2013). Third, a frequency-based reconstruction method was applied to the historical documents to improve their ability to reflect the historical extreme events (Zheng et al. 2014a). An objective extrapolation method was then used that is based on the teleconnections between the precipitation in East China and other remote regions. Fourth, to better avoid signal aliasing (Shi et al. 2013), instead of directly compositing the tree rings and historical documents, we performed two individual reconstructions first, and then combined them into one dataset by a "correlation skill–based weighting" method. Last, we establish the weighting models using the data before 1950, during which the historical documentary records are largely free of the impact of instrumental data so that the impact of instrumental data on the weighting process is minimized.
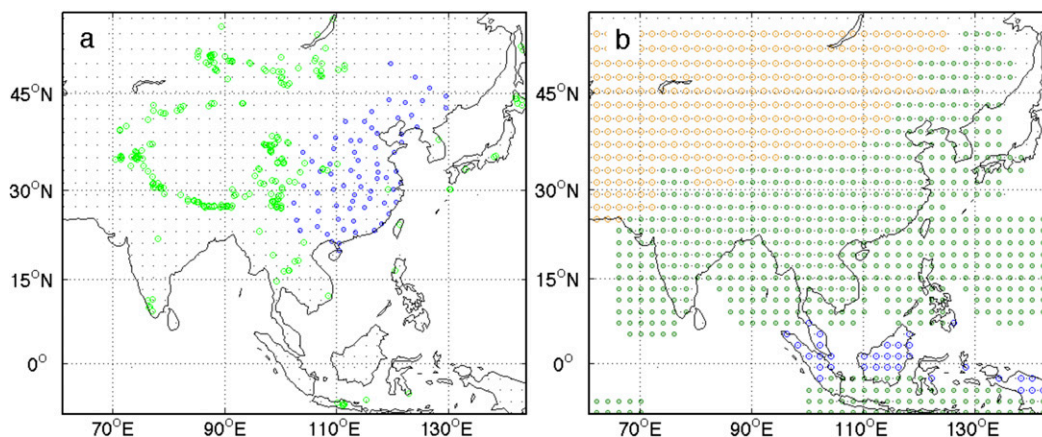
FIG. 1. (a) Research domain with locations of the 453 tree-ring chronologies (green dots) and 71 historical documentary records (blue dots). (b) Monsoon Asia (dark green), arid Asia (dark yellow), and the MC (blue). The monsoon Asia domain is defined by the following criteria: annual range of precipitation exceeds 300 mm (or 2 mm day^{-1}) and local summer (MJJAS) precipitation exceeds 55% of the annual total precipitation (Wang and Ding 2008). The region to the northwest side of the monsoon domain is considered to be the semiarid/arid region.

Section 2 describes how the reconstructed Asian summer precipitation (RAP) dataset is generated, including descriptions of the tree rings and historical documents used, and the reconstruction methods. In section 3, the RAP dataset is verified against independent instrumental data from the Climatic Research Unit (CRU; Harris et al. 2014) for the early twentieth century and the long-term instrumental precipitation records that go back to the 1770s (Seoul, South Korea) and 1810s (India). Section 4 presents an intercomparison between the RAP and other proxies before the instrumental period, including speleothem records, ice-core records, and a marine upwelling record. The RAP climatology and large-scale interannual–decadal variability during the twentieth century are also compared with the results derived from another observed dataset compiled by the Global Precipitation Climatology Centre (GPCC; Schneider et al. 2015; section 4). The leading modes of variability of the RAP are examined in section 5. Discussions (section 6) and conclusions (section 7) are then presented.

2. Reconstruction of the Asian summer precipitation: Data and methods

The reconstruction domain is shown in Fig. 1 (from 8.75°S to 55.25°N, and from 61.25°E to 143.25°E), covering the South Asian and East Asian monsoon subsystems, the "Maritime Continent" (MC), and semiarid/arid central Asia. The summer [June–August (JJA)] precipitation was reconstructed with an annual temporal resolution and a 2° by 2° spatial resolution. The datasets used for reconstruction and their temporal spans are shown in Fig. 2.

a. The historical documentary records and reconstruction method

The historical documentary records we used are flood/drought-level-coded data in East China dating back to 1470 (1470–2003; Fig. 2). The level-coded data were derived from a 500-yr flood/drought atlas, which was originally defined by five levels: severe flood, flood, normal, drought, and severe drought (Wang and Zhao 1979). Li et al. (2005) added two more levels, that is, extreme flood and extreme drought, by going through local chronicles for extreme climate events, which occur once in 30 years. Seventy-one stations (blue dots in Fig. 1a) were selected because they have relatively long precipitation records and are almost evenly distributed across East China (Wang et al. 2000; Li et al. 2005).

The key to reconstructing precipitation from historical documentary records lies in the occurrence frequencies of the seven drought/flood levels, which are 0.033, 0.100, 0.233, 0.268, 0.233, 0.100, and 0.033. We used observed JJA mean precipitation over 1951–89 as a reference. For each station location, the 39-yr rainfall series was ordered from maximum to minimum and binned into seven groups to obtain similar frequencies of occurrence mentioned above (i.e., order number 1, 2–5, 6–14, 15–25, 26–34, 35–38, and 39, respectively). For each group, precipitation is then averaged to represent the rainfall amount of the corresponding drought/flood level. With this transformation, annual summer precipitation amount was estimated for the level-coded data and extended back to 1470.

To extend the reconstruction from East China onto the whole Asian domain, we applied an objective extrapolation method that is based on the teleconnections
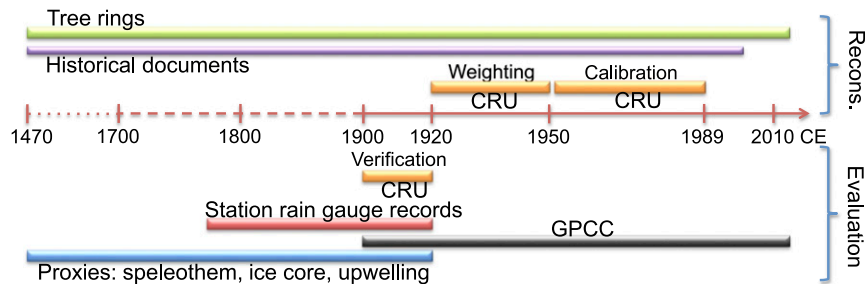
FIG. 2. Data used for reconstruction and evaluation.

between precipitation in East China and other remote regions and using stepwise regression. The high-resolution gridded monthly precipitation product CRU Time Series (TS) 3.22 is used for extrapolation. For each grid point outside East China, we correlated the local CRU precipitation series with the 71 time series in East China from 1951 to 1989 (Fig. 2). We selected significantly correlated time series above the 80% confidence level ($p < 0.2$, 2 tailed) as potential "predictors," because the resultant extrapolation was most satisfactory among sensitivity test results for various significance levels. We then applied stepwise multiple linear regression with these predictors. Stepwise regression is a systematic method for adding and removing predictors from a multivariable linear regression model based on the statistical significance of their contributions to the overall variance explained by the model (Draper and Smith 1998). We chose the maximum p value for a predictor to be added as 0.05, and the minimum p value for a predictor to be removed as 0.10. Through these procedures, we extended the precipitation series in East China both temporally and spatially to the entire study domain for the past five centuries.

Such extrapolation is not merely a statistical remedy; it does have its physical basis. For instance, there is a robust linkage in summer precipitation among northern East China, India, and the MC. Using 116-yr GPCC data (1901–2016), the northern East China summer precipitation has a significant correlation with that over India (correlation coefficient $r = 0.38$; significance level $p < 0.05$) and the MC ($r = 0.49$; $p < 0.05$). The stalagmite records from Wanxiang Cave in northern East China and from Dandak Cave in central India are shown to vary coherently (Berkelhammer et al. 2010), although there is the ambiguity in the meaning of the speleothem records (e.g., Tan 2016; Chen et al. 2016). Here we assume that the relationship in summer precipitation between East China and other regions is stable over time.

b. The tree-ring network and reconstruction method

The tree-ring network we used was achieved through collective effort of many tree-ring scientists over

decades in developing climatically sensitive tree-ring chronologies in the AM region (e.g., Shao et al. 2005; Li et al. 2006; Fang et al. 2010; Gou et al. 2015; Cook et al. 2010; Yang et al. 2013b). An updated version with a total of 453 tree-ring chronologies was used for the reconstruction (Cook 2015; Cook et al. 2013). The earliest starting point of the tree-ring series is AD 150, and the common (i.e., earliest) last year of the series is 1989, with most of them clustered after 1500. The spatial coverage of the network is limited because of the intrinsic availability of trees and limited accessibility of existing tree-ring chronologies. For example, over central Asia, parts of western China, and the Tibetan Plateau, no forest cover can be found; in lowland tropics, only a few tree species are suitable to sample. It was suggested that a screening procedure for tree-ring chronology is necessary for quality control, because not all of them respond well to the precipitation change in China (Shi et al. 2017). However, some studies have shown that screening may provide artificial skill (e.g., DelSole and Shukla 2009). Therefore, we did not perform screening before the reconstruction.

We used the tree-ring-width chronologies and applied the "point-by-point regression" method (PPR; Cook et al. 1999). PPR is a well-tested principal components regression method and has produced high-quality drought reconstruction over North America (Cook et al. 2007) and over the AM region (Cook et al. 2010). PPR is based on the proposition that only tree-ring chronologies relatively close to a given grid point are likely to have a stable relationship with the climate variables at that location, thus are likely to be true "predictors." Because of the limited spatial coverage of the tree-ring network over Asia, to find the minimum amount of tree-ring series (here set to 10) for each grid point requires a much larger search radius than the e-folding distance (i.e., 490 km; Fig. S1 in the online supplemental material) of the precipitation correlation decay. Greatly expanded search radii from 500 up to 3800 km were used in reconstructing the summer monsoon precipitation. This is similar to what was done in
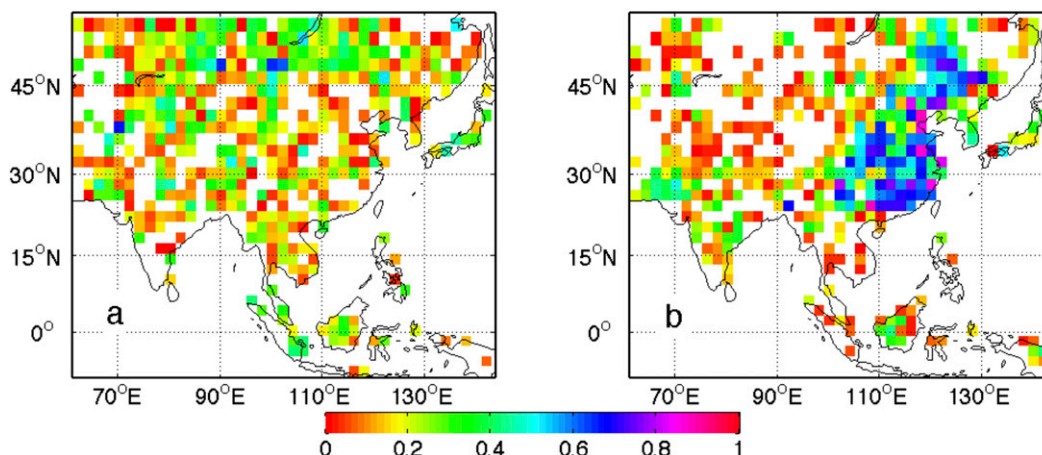
FIG. 3. Weights assigned to (a) the tree-ring-based and (b) the historical-document-based reconstructions according to the correlation coefficients between the reconstructed and CRU (Harris et al. 2014) precipitation from 1921 to 1950. Only positive correlations are plotted. Equal weights are applied in rare cases in which neither reconstruction has a positive correlation.

producing the MADA (Cook et al. 2010). We assumed that, over broad areas with relatively low topographic complexity such as the Tibetan Plateau and the Mongolian steppes, meaningful correlations can be found between tree rings and climate. In areas where no trees were available, such as in East China and the Tarim basin in western China, the adjacent tree rings can, to some degree, extrapolate over the void and provide useful climate information.

The calibration data we used are monthly precipitation from CRU TS 3.22. The calibration period was chosen from 1951 to the common last year of the tree-ring series, that is, 1989 (Fig. 2) because the data quality of this time period is relatively high as compared with that before 1950 (Cook et al. 2010). The output is 2° by 2° gridded summer precipitation with full coverage of the Asian land region dated back to 1300.

c. Method to combine the two reconstructions

To combine the precipitation reconstruction from tree-ring chronologies and that from historical documents into one unified dataset, we applied a correlation skill–based weighting method. We argue that in the region where one reconstruction has a higher correlation with observation, this reconstruction should be given a higher weight.

As discussed at the beginning, the historical level-coded data are not homogeneous. For the 71 historical documentary records used in this study, the levels were determined solely with instrumental precipitation after 1950. From 1900 to 1950, however, the percentage of instrumental data involved in determining the levels is significantly lower (~34%; Wang et al. 2000). Therefore,

we use the period from 1921 to 1950 as the weighting period (Fig. 2). By doing so, the bias toward putting higher weights on the historical documents can be best prevented. Only positive correlations are selected for determining the weights. As such, only grid points with positive correlations are used as candidates to enter the weighting. In rare cases when both correlations are negative for both reconstructions, we applied equal weights.

As we expected, the weights for the tree-ring-based reconstruction and for the historical-document-based reconstruction largely complement each other (Fig. 3), although the highest weights are still found for the historical-document-based reconstruction over East China where the original historical documents are obtained (Fig. 3b). Relatively high weights are also found over western and southern India, showing the teleconnection between the rainfall in East China and in western India. In addition, high weights are found in the northern part of northeastern China, in the northern part of the Indochina Peninsula, and in west Borneo for the historical-document-based reconstruction. For the tree-ring reconstruction, higher weights are found in other geographic regions (Fig. 3a), where tree-ring samples are incorporated. These regions include Siberia northeast of Kazakhstan, Mongolia, and Hokkaido, Japan; Tajikistan, Kyrgyzstan, north Pakistan, and north India; south of the Himalayas including Nepal, Bhutan, Bangladesh, northeast India, and the western part of Xinjiang Uygur, China; and the Indochina Peninsula, Malay Peninsula, Sumatra, and west Borneo.

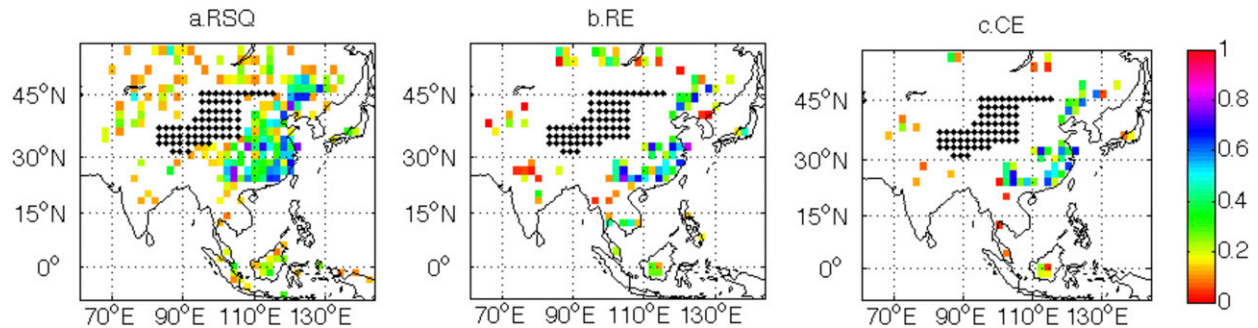The combined reconstruction at each grid can be achieved through the following equation:

FIG. 4. Verification statistics for the RAP against CRU from 1901 to 1920. (a) For RSQ, only correlations that are higher than the 90% significance level (1 tailed) are shown. (b) The RE and (c) CE, regions with positive skill are shown (RE > 0; CE > 0). Black-dotted areas are missing values in the CRU dataset during this time period.

$$\mathrm{RECONS_{combined}} = \mathrm{RECONS_{tr}} \times \frac{\mathrm{cor_{tr}}}{\mathrm{cor_{tr} + cor_{hist}}}$$
$$+ \mathrm{RECONS_{hist}} \times \frac{\mathrm{cor_{hist}}}{\mathrm{cor_{tr} + cor_{hist}}},$$

where $\mathrm{RECONS_{combined}}$, $\mathrm{RECONS_{tr}}$, and $\mathrm{RECONS_{hist}}$ represent combined reconstruction, tree-ring-based reconstruction, and historical-document-based reconstruction, respectively. The variables $\mathrm{cor_{tr}}$ and $\mathrm{cor_{hist}}$ denote the correlation coefficients of the tree-ring-based and historical-document-based reconstruction with CRU data for the period from 1921 to 1950, respectively. The assumption for this combination is that the weights determined by the period from 1921 to 1950 are also valid for years before 1921.

3. Verification of the reconstructed Asian summer precipitation

a. Verification of the RAP against CRU (1901–20) data

The RAP was verified against the CRU precipitation anomalies for the 1901–20 period. The reason for selection of this short period is that data from 1950 to 1989 were used for calibration and the data from 1921 to 1950 were used to determine the weight of merging the two reconstructions (Fig. 2). The large-scale instrumental precipitation data are available only after 1901. The calibration and weighting processes left only the period from 1901 to 1920 for out-of-sample verification.

The reconstruction skill was evaluated using the standard statistical significance testing, which have been frequently used in previous studies for reconstruction verification (Cook et al. 2010; Feng et al. 2013; Shi et al. 2017). They include the square of the Pearson correlation coefficient (RSQ) between observation and reconstruction during the

verification period, reduction of error (RE), and the coefficient of efficiency (CE). RE and CE are calculated as

$$\mathrm{RE} = 1.0 - \left[\frac{\sum (x_i - \hat{x}_i)^2}{\sum (x_i - \overline{x}_c)^2} \right] \quad \text{and}$$

$$\mathrm{CE} = 1.0 - \left[\frac{\sum (x_i - \hat{x}_i)^2}{\sum (x_i - \overline{x}_v)^2} \right],$$

respectively. The variables $\overline{x}_c$ and $\overline{x}_v$ are the means of observation during the calibration and verification period, respectively. The variables x_i and $\hat{x}_i$ are the observed and reconstructed values during the verification period, respectively. RE determines if the reconstruction is better than the climatology of the calibration period, with RE > 0 indicating positive skill of reconstruction. The CE is similar to RE but the values are smaller than RE when $\overline{x}_c \neq \overline{x}_v$. Thus, it is more difficult to pass the test with CE > 0 for skillful reconstruction.

Relatively good agreement, with RSQ higher than 0.16 ($p < 0.1$, 1 tailed), albeit sparse, is found in East and North China, southern Japan, Mongolia, Siberia northeast of Kazakhstan, north Pakistan, and north India, and over the MC, including Borneo, Malay Peninsula, and south Sumatra (Fig. 4a). However, over various parts of India, regions south of the Tibetan Plateau, and parts of the Indochina Peninsula, the RSQ is largely insignificant (Fig. 4a). The RE in Fig. 4b shows skillful reconstruction in East and North China, the Indochina Peninsula, the MC, northern India and Pakistan, midlatitude Asia, and southern Japan. The CE (Fig. 4c) shows similar spatial distribution of skill, but the magnitudes are lower than that of RE.

We also examined individual reconstructions with single-type proxy to evaluate by how much the merged reconstruction has improved the skill. Standard verification statistics are applied to reconstructions with only
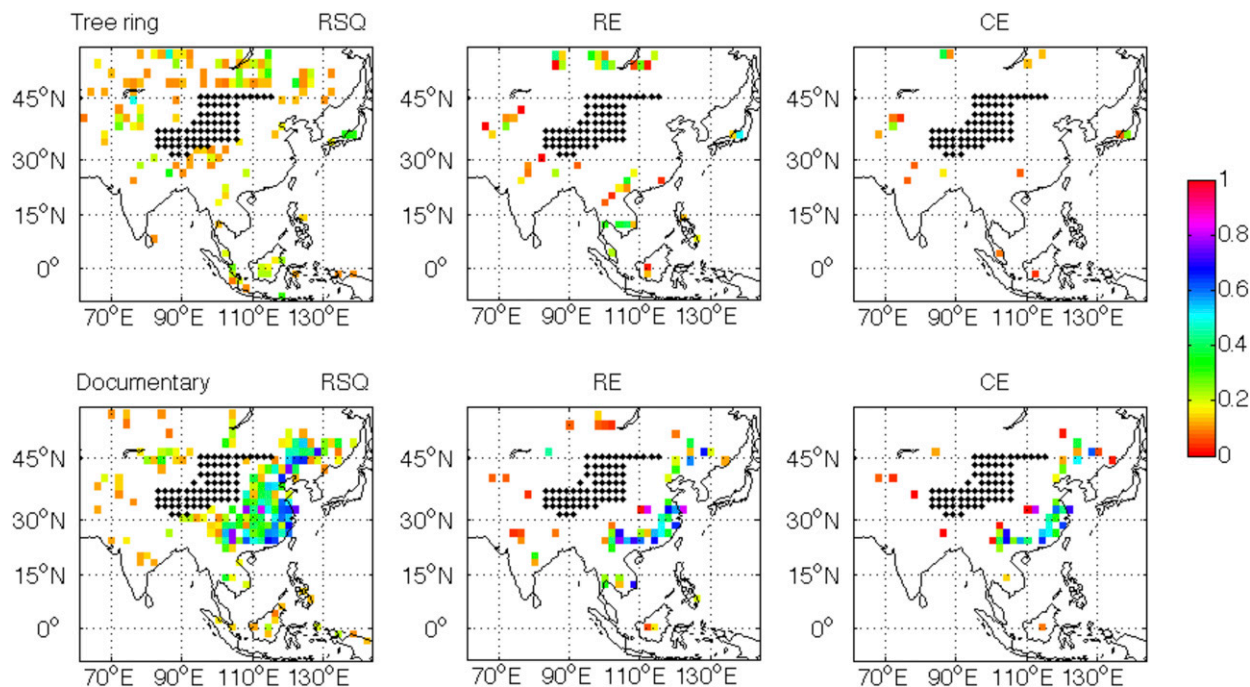
FIG. 5. As in Fig. 4, but for reconstructions from (top) only tree rings and (bottom) only historical documents.

tree rings and only historical documents, respectively (Fig. 5). The reconstruction with only tree rings shows skill over midlatitude Asia, central Asia, northern India, the Indochina Peninsula, the MC, and southern Japan (Fig. 5, top). The reconstruction with only historical documents shows skill over East China, north-central India, and the southern Indochina Peninsula (Fig. 5, bottom). The RSQ of the two individual reconstructions are largely complementary with each other. Although the RSQ from tree-ring records is relatively small relative to that produced by documentary records, the combination of the two is shown to have improved reconstruction skill over most of the AM region (Figs. 4 and 5).

b. Verification against long-term instrumental data before 1920 (1771–1920)

We further verified the RAP against long-term instrumental records (Fig. 2). One example of such records is the Indian Institute of Tropical Meteorology Indian regional/subdivisional monthly rainfall dataset dating back to 1813 (Sontakke et al. 2008). This "all India" record comes from an extensive network of rain gauge stations and is area weighted for India. Another record is from Seoul (37°N, 126°E), which is one of the world's longest instrumental measurements of daily precipitation since 1771 (e.g., Wang et al. 2006). This record was compiled from ancient rain-measuring devices used during the Chosun Dynasty, as well as modern rainfall observations since 1908.

General agreement is found between the RAP and the long-term rain gauge records (Table 1). The 108-yr all-India record shows significant positive correlation ($r = 0.2$; $p = 0.02$) with the reconstruction outside of the calibration period. Within India, significant correlations are found over most subregions except northeast India and the southern peninsula. The highest correlation is found in the north-central region ($r = 0.32$; $p < 0.1$), followed by eastern ($r = 0.30$; $p < 0.1$), and western peninsula regions ($r = 0.28$; $p < 0.1$). In Seoul,

TABLE 1. Correlation coefficients between the RAP and long-term instrumental records. Numbers in parentheses are correlations for the common period 1848–1920. Boldface numbers are statistically significant at the 90% confidence level ($p < 0.1$, 1 tailed). The area for each index is determined on the basis of the definition of each subregion in India (Sontakke et al. 2008, their Fig. 1), and the location of the record in Seoul.

| Regions or subregions (indented)	Time period	Correlation coef
All-India	1813–1920	**0.22 (0.30)**
North mountainous India	1844–1920	**0.21 (0.21)**
Northwest India	1826–1920	**0.19 (0.26)**
North-central India	1831–1920	**0.26 (0.32)**
Northeast India	1829–1920	0.09 (0.05)
West peninsula India	1817–1920	**0.24 (0.28)**
East peninsula India	1848–1920	**0.30**
South peninsula India	1813–1920	0.02 (0.03)
Seoul	1771–1920	**0.18** (0.11)
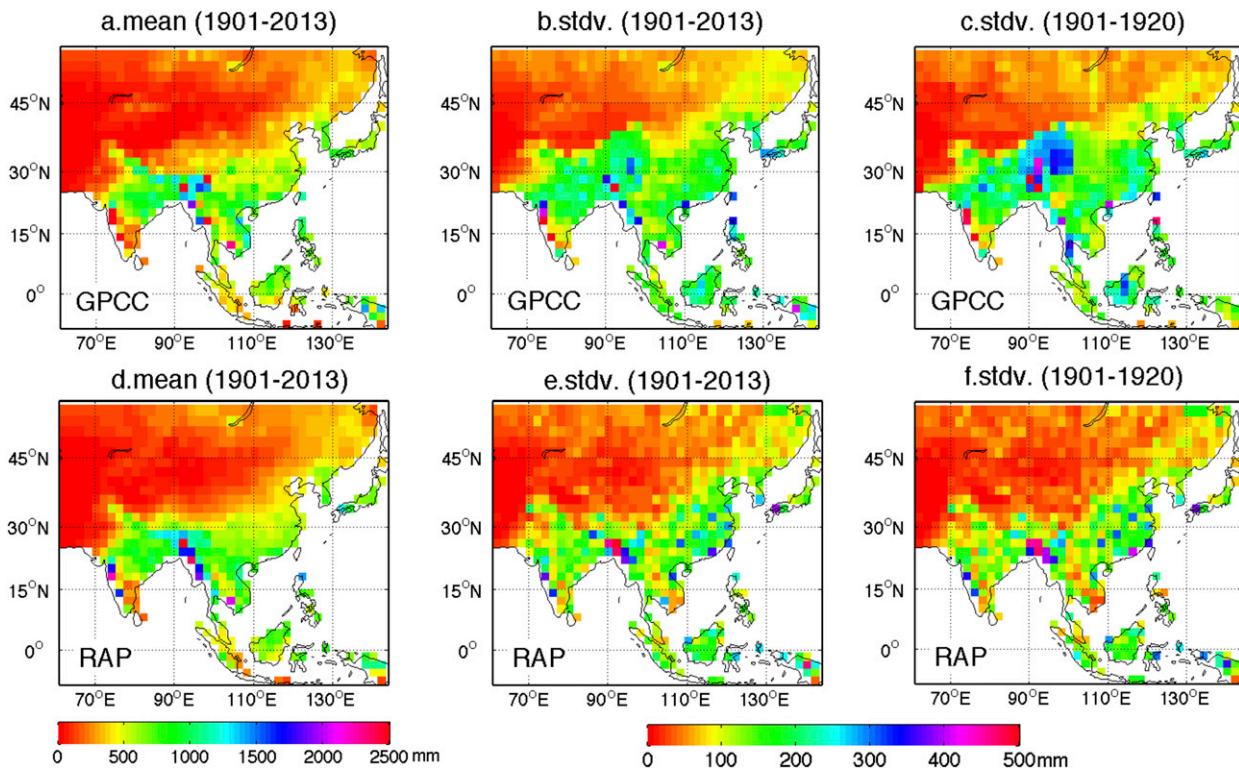
FIG. 6. Twentieth-century climatological mean and standard deviation for the GPCC and the RAP.

the correlation coefficient is 0.18 ($p = 0.03$), which is reasonably good given that the Seoul record is a single station observation and is the longest time span of the records from 1771 to 1920.

c. Sensitivity to parameter choices

As described in section 2, a relatively short weighting period (30 years; 1921–50) was used for combining the two reconstructions (Fig. 2). This is constrained by the data availability. The special property of the historical documentary records requires a weighting model built with data prior to 1950, while the out-of-sample verification requires withholding of data. Therefore, we reserved the available CRU data during 1901–20 for the out-of-sample verification. To test to what extent the low-frequency variability of the precipitation is captured with this short weighting-training period, a reconstruction with a longer weighting period (LONG), from 1901 to 1950, is fashioned to compare with this reconstruction (SHORT). The area-weighted index averaged over all of Asia from LONG is significantly correlated with that from SHORT ($r = 0.99$; $p < 0.05$). In terms of the periodicity, power spectra of the area-weighted indices averaged over Asia from both LONG and SHORT are shown to have preserved low-frequency variability, and the locations

of all low-frequency peaks are the same (Fig. S2 in the online supplemental material).

Another possible concern is the choice of targeted season of reconstruction. Two previous reconstructions (Shi et al. 2017; Feng et al. 2013) both aim at warm-season [May–September (MJJAS)] rainfall. The reason why we chose the JJA mean precipitation is based on Wang and Zhao (1979). They compared the leading empirical orthogonal function (EOF) modes using 508-yr drought/flood indices from 25 stations located in East China with observed summer precipitation (24 years) from 100 weather stations and found that the spatial patterns of the variability modes are very similar. They concluded that the drought/flood indices could reflect the summer precipitation variability in East China. We conducted sensitivity tests to compare the reconstructed JJA precipitation variations with the MJJAS precipitation variability. The area-weighted index averaged over all of Asia from JJA reconstruction accounts for almost one-half (46%) of the total variance of MJJAS rainfall. The correlation coefficient between the JJA and MJJAS indices reaches 0.94 ($p < 0.05$), indicating that, at least on a large spatial scale, the JJA precipitation variations could largely reflect the MJJAS precipitation variability in the research domain.
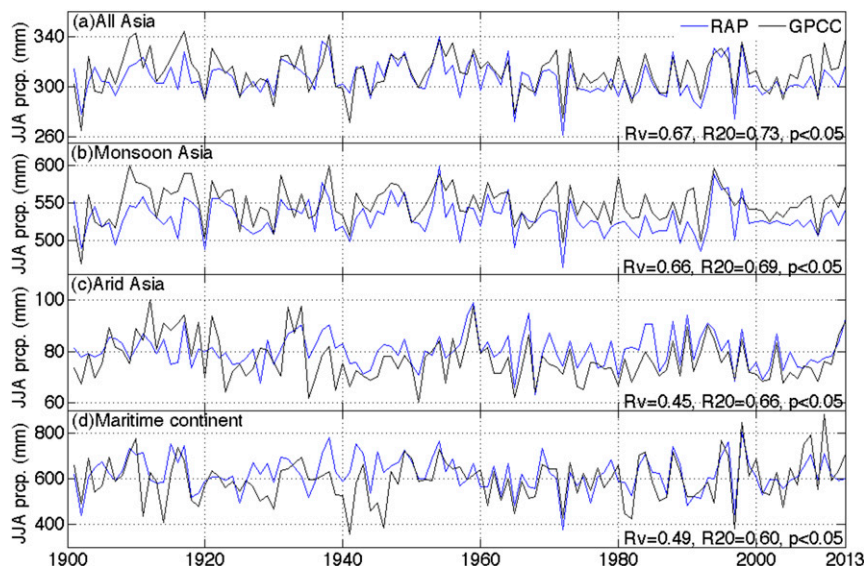
FIG. 7. Comparison of the area-weighted precipitation indices derived from the RAP (blue) and GPCC (black) for (a) all Asia, (b) monsoon Asia, (c) arid Asia, and (d) the MC; Rv is the correlation coefficient during the verification period (1901–20), and R20 is the correlation coefficient during the twentieth century.

4. Further evaluation of the RAP

a. Intercomparison between the RAP and GPCC climatology and large-scale precipitation indices

The RAP climatology was compared with that derived from the GPCC monthly precipitation dataset from 1901 to present (Fig. 2). As shown in Fig. 6, the climatological mean of the reconstruction (Fig. 6d) resembles that from the corresponding observation (Fig. 6a) with a pattern correlation coefficient (PCC) of 0.89. The standard deviation from the RAP (Fig. 6e) is overall less in amplitude compared with that from the observation (Fig. 6b), especially over the Indochina Peninsula and the Tibetan Plateau, but the PCC between the two is reasonably good (0.76). However, for the verification period, the discrepancy over the Tibetan Plateau increases (Figs. 6c,f), and the PCC drops to 0.57.

Large-scale precipitation variability is represented by area-weighted mean RAP indices in Fig. 7. Over all Asia, the reconstructed Asian precipitation index is significantly correlated with that from the GPCC, with a correlation coefficient of 0.73 ($p < 0.05$) for the twentieth century and 0.67 ($p < 0.05$) for the verification period (1901–20; Fig. 7a). The Asian domain was further divided into monsoon Asia, arid Asia, and the MC (Fig. 1b). The definition of monsoon domain follows Wang and Ding (2008).

For monsoon Asian precipitation index, the correlations are consistently high: 0.69 ($p < 0.05$) for the twentieth century and 0.66 ($p < 0.05$) for the verification

period of 1901–20 (Fig. 7b). The high correlation in monsoon Asia is likely attributed to the inclusion of abundant historical records in East China (Fig. 1a). For arid central Asia, the area-weighted mean precipitation index shows a fairly good relationship with the observed counterpart with $r = 0.66$ ($p < 0.05$) for the twentieth century and $r = 0.45$ ($p < 0.05$) for the verification period. This indicates that tree rings and teleconnections have contributed to the RAP's improved representation of the rainfall variability outside the historical record–dense region in East China. Slightly lower, albeit significant, correlations are found over the MC ($r = 0.60$; $p < 0.05$), which is possibly due to lack of proxy samples. These results suggest that the RAP can effectively capture large-scale rainfall variability in different parts of Asia during the twentieth century. Yet the skill varies over the study region because of the differences in proxy coverage, proxy type, and the extent to which the climatological regime is driven in the region by large-scale factors.

b. Intercomparison between the RAP and other proxies during 1470–1920

To evaluate the quality and reliability of the reconstruction before 1920, we further compared the RAP with various published monsoon proxies, including eight speleothem $\delta^{18}O$ records from caves across the AM region, three ice-core records from the central Himalayas and Tibetan Plateau region, and one upwelling record from the Arabian Sea (Fig. 2). Speleothem $\delta^{18}O$ series have been used as proxies of monsoon variability in

Asia, and negative correlations are expected between speleothem $\delta^{18}O$ series and precipitation anomalies (e.g., Xu et al. 2013, 2015; Gou et al. 2015; Tan et al. 2015). Ice-core records have been shown to reflect past climatic conditions and large climate events, as well as temperature and moisture variability (Thompson et al. 2006a). Monsoon intensity changes in particular have been associated with ice-core dust and chloride concentrations, aerosol history, and snow accumulation (Thompson et al. 2000; Duan et al. 2004; Thompson et al. 2006b). In this study, we used the most straightforward variable, which is the snow accumulation (Thompson et al. 2000; Duan et al. 2004), and positive correlations are expected with the monsoon reconstruction. For each proxy record, a 5 by 5 grid box centered at the location of the proxy is selected to calculate time series with the RAP. The size of the box is determined on the basis of the correlation decay e-folding distance, which is 490 km (roughly 2.2 of the $2°$ grids). Pentad time series (average over every 5 yr) from 1470–1920 are used to examine relationships on the decadal time scale.

The RAP shows overall agreement with speleothem and ice-core records on decadal time scales, where reddish colors indicate negative (positive) correlation with speleothem (ice-core series) (Fig. 8). Eighty-three percent of all grid points show significant agreement ($p < 0.2$, 1 tailed) with the other proxies. In comparison, the percentage of grids in agreement with proxies is 66% for the tree-ring-only reconstruction and 76% for the historical-document-only reconstruction (Fig. S3 of the online supplemental material), indicating an improvement of fidelity of the combined RAP. Agreement is found for most of the adjacent areas of all eight caves in central and northwest China and India and three ice cores located in the central Himalaya and the Tibetan Plateau (Fig. 8). However, discrepancies remain in several places, including north of Kesang Cave in northwestern China, near Dongge Cave in south China, near Guliya in the western Tibetan Plateau, and near Dasuopu ice cores in the central Himalayas.

The RAP was also compared with a 1000-yr upwelling proxy record from the Arabian Sea (Anderson et al. 2002). The upwelling record is interpreted as a low-frequency (50-yr interval) Asian southwest monsoon index, which shows that the monsoon upwelling reached a minimum around 1600 and increased thereafter with a relatively rapid rate to around 1700. The low-frequency variations of the RAP show a salient strengthening of the Indian summer monsoon (ISM) that had occurred during 1630–70 (Fig. 9a). Before this increase at the turn of 1600, strong dry anomalies are shown over India, especially over western-peninsula
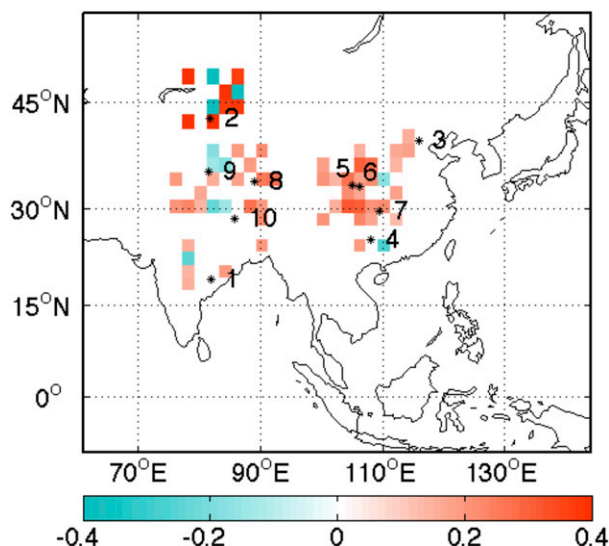

FIG. 8. Comparison of the RAP and proxy data. Shown are the correlation coefficients between the RAP and proxies (speleothem $\delta^{18}O$ records and ice-core snow-accumulation records) for the period of 1470–1920. Only significant correlations above the nominal 80% confidence level (2 tailed) are shown. Note that the correlations between the RAP and speleothem are multiplied by −1. The cave or ice-core names corresponding to the number labels are Jhumar and Dandak (cave 1; Sinha et al. 2011), Kesang (cave 2; Cheng et al. 2012), Shihua (cave 3; Li et al. 1998), Dongge (cave 4; Y. Wang et al. 2005), Wanxiang (cave 5; Zhang et al. 2008) and Huangye (cave 5; Tan et al. 2011), Dayu (cave 6; Tan et al. 2009), Lianhua (cave 7; Cosford et al. 2009), Puruogangri (core 8; Thompson et al. 2006b);, Guliya (core 9; Thompson et al. 1997); and Dasuopu (core 10; Thompson et al. 2000).

India during the period of 1580–1630 (Fig. 9b). The time series of the area-averaged summer rainfall over India (Fig. 9c) further illustrates the multidecadal changes of the ISM during the past 500 years. It is noted that rainfall in northern East China also strengthened as the ISM increased (Fig. 9a). During the dry phase of the ISM, other parts, including south-central China, northern East China, and the MC also experience dry conditions (Fig. 9b).

5. Leading modes of the year-to-year variability of the RAP

To examine the long-term variability of the Asian summer precipitation, we utilized the full span of the RAP dataset. An EOF analysis is applied to the yearly RAP data after spatial smoothing, area weighting, and standardization (Figs. 10 and 11). The linkages of the principal components (PCs) with global sea surface temperatures (SSTs) are examined to understand their origins (Fig. 12). The SST data used are from the Hadley Centre Sea Ice and Sea Surface Temperature dataset (HadISST; Rayner et al. 2003) from 1870 to 2013.
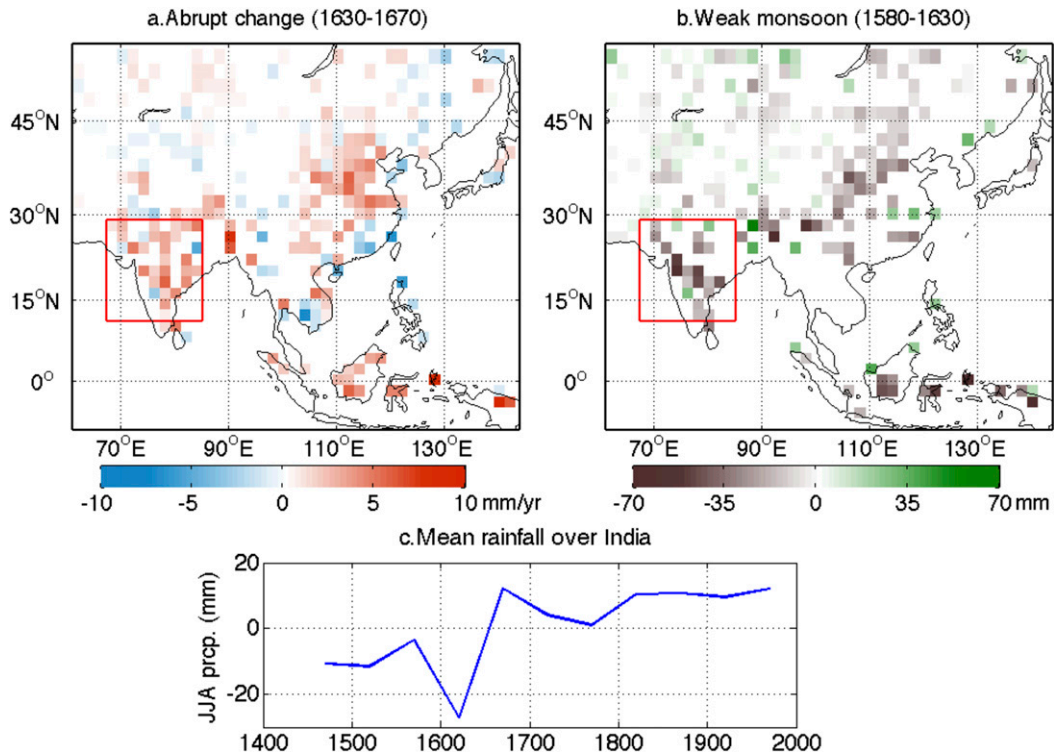
FIG. 9. (a) Linear trends during 1630–70, and (b) summer precipitation anomalies during 1580–1630 derived from the RAP dataset. Only significant trends/anomalies above the 80% confidence level (2 tailed) are plotted. Also shown is (c) 50-yr smoothed summer precipitation averaged over India [red-outlined box in (a) and (b)].

The first EOF mode shows a generally uniform drying pattern over most parts of the AM region, including India, East China, and the MC (Fig. 10a). It explains 17.4% of the total variance. The PC1 is correlated with a La Niña–like cooling pattern in the preceding winter (Fig. 12, first column), which disappears during the spring, and from summer to the following winter an El Niño–like SST pattern develops, suggesting that the unified drying pattern is associated with the eastern Pacific Ocean El Niño–developing process, or a transition from a cold phase to a warm phase of ENSO. Spectral analysis indicates that PC1 has significant peaks ranging from 2 to 3 years (Fig. 11), reflecting its association with the biennial or high-frequency component of ENSO (Fig. 12, first column). This mode can be properly identified as a biennial ENSO mode.

In comparison, EOF4 is also found to be associated with eastern Pacific El Niño events (Fig. 12, fourth column). The difference is that during the preceding winter the ocean conditions are El Niño–like rather than La Niña–like and that the eastern Pacific warming is long lasting throughout the year until the following winter. The spectrum of PC4 shows a pronounced 5-yr peak that passes the 95% significance level, reflecting its association with the low-frequency component of ENSO

(Fig. 11), as reflected by the relatively slow development of El Niño (Fig. 12, fourth column). Therefore, this mode is identified as the low-frequency ENSO mode. Drying over India and the Indochina Peninsula is observed, and a quadrupole pattern over East Asia is found (Fig. 10d).

EOF3 shows a tripole pattern over the East Asian land, and drying over western China and the north of India (Fig. 10c). It explains 8.7% of the total variance. The PC3 is associated with the central Pacific (CP) warming that develops from the summer and sustains to the winter (Fig. 12, third column). The major periodicity of PC3 is around 9 years (Fig. 11). We identify this mode as a CP El Niño–like decadal mode.

EOF2 has a strong loading over the Yangtze River valley (YRV) where the major subtropical frontal zone is located and over South China. Loadings of the opposite sign are found over India, Pakistan, and northeastern Asia (Fig. 10b). It explains 12.9% of the total variance. This mode does not seem to relate with ENSO (Fig. 12, second column). Rather, PC2 is significantly correlated with anomalous SSTs over the Indian Ocean and midlatitude North Pacific Ocean (Fig. 12, second column). The spectrum of PC2 shows very strong peaks in the 20- to 50-yr periods (Fig. 11). Thus, we conclude
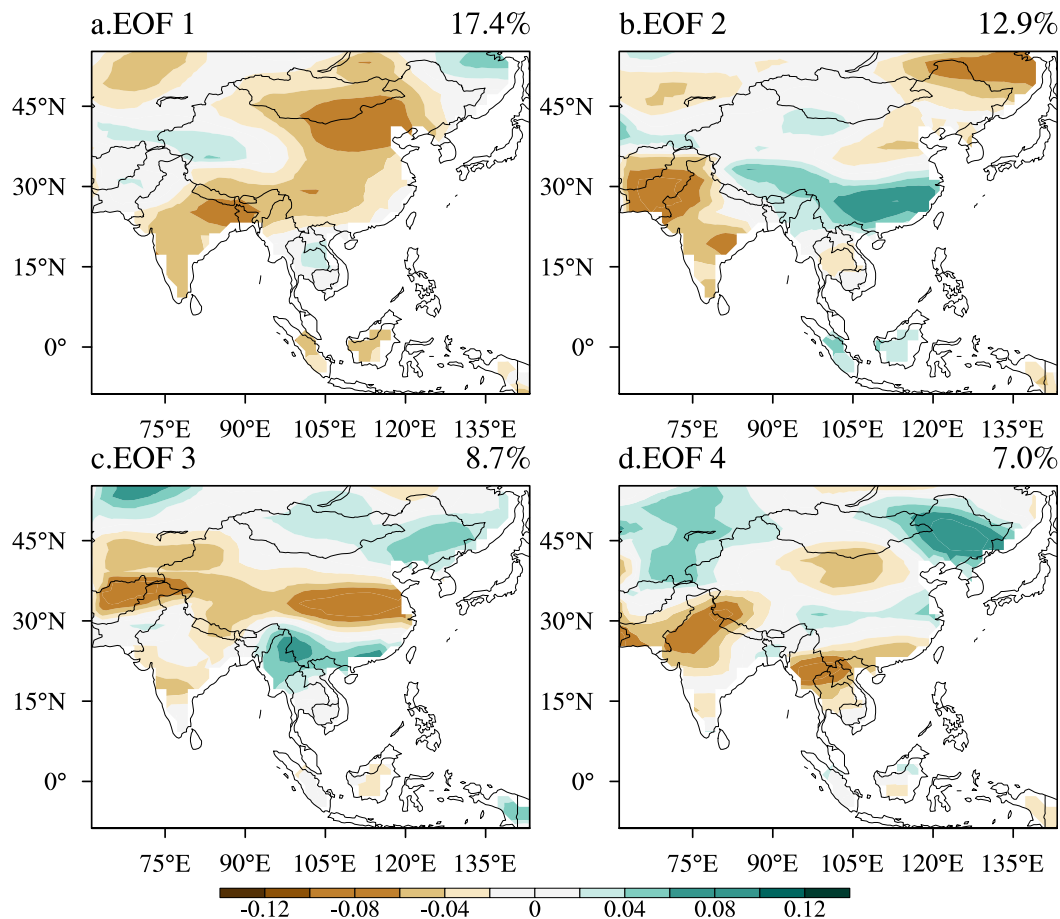
FIG. 10. Spatial patterns of the leading EOFs of the RAP.

EOF2 is an interdecadal mode that is likely associated with oceanic low-frequency variability modes. The behavior of the major modes of variability revealed from the RAP will be compared with those derived from other reconstructions in the next section.

6. Discussion

While the RAP represents large-scale precipitation anomalies with fidelity, its uncertainty increases toward small and local scales. Major uncertainties of the RAP exist over central Asia, southern and northeastern India, and regions south of the Tibetan Plateau (Fig. 4). For central Asia, uncertainty is partially due to the reduced quality of the CRU data (Cook et al. 2010, 2013) and lack of observations in this area before 1920 (Fig. 4). For regions including southern and northeast India, Nepal, and Bangladesh, the high uncertainty of the reconstruction is likely due to a combination of lack of trees, low teleconnection with other parts, and high variability of local rainfall related to the vigorous air–sea interaction over the Bay of Bengal and topography.

Therefore, local and small-scale rainfall anomalies derived from the RAP should be interpreted with caution.

There is some degree of mismatching between the reconstruction and other proxies (Fig. 8). The mismatching with the speleothem record could be partially due to the obscure interpretation of the climate meaning of the oxygen isotope from the speleothem records that are raised in recent studies (e.g., Chen et al. 2016; Tan 2016). The disagreement with the ice-core record could arise from multiple sources. For instance, the ice-flow dynamics could affect snow accumulation in ice-core records (Thompson et al. 2000), and uncertainties associated with age models and dating methods in ice-core records could also contribute to the disagreement (Clemens 2006).

The RAP agrees with the upwelling record on the timings of weak ISM and the rapid ISM strengthening (Fig. 2 in Anderson et al. 2002). A similar increase is also found in speleothem records from central India (Sinha et al. 2011). The duration of the monsoon-increasing period shown in the RAP (40 years) is shorter than that shown in the upwelling record (about a century),
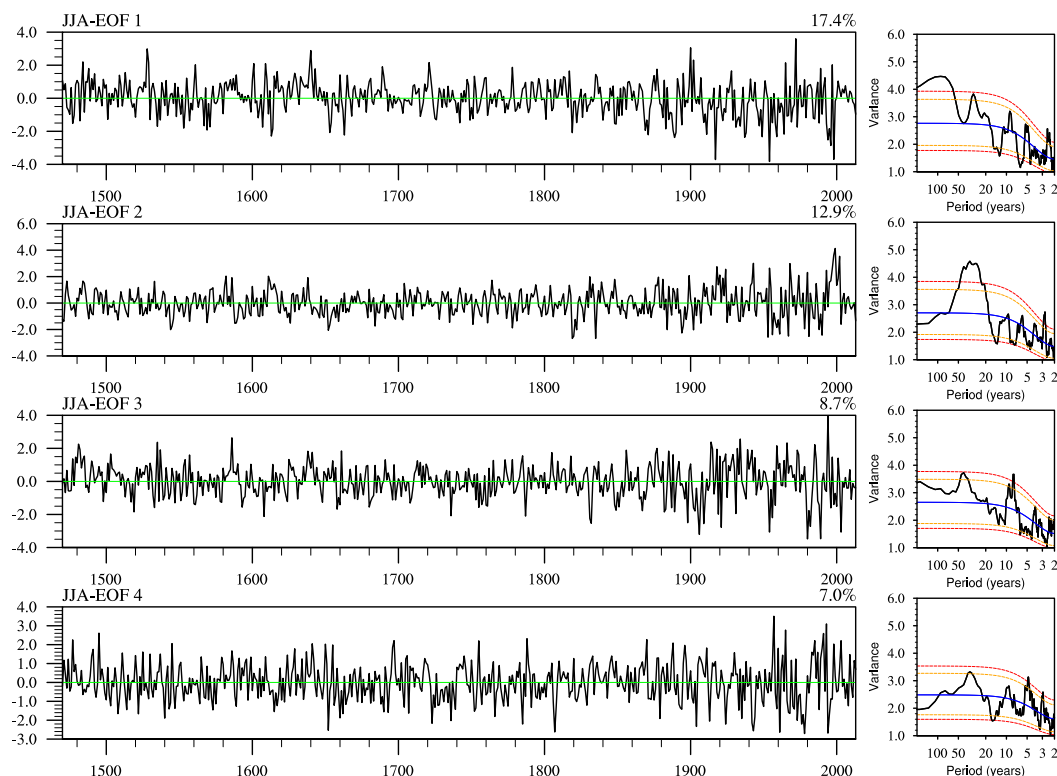
FIG. 11. The PCs and their power spectra derived by using forward fast Fourier transformation, with 10% of the data tapered, and the modified Daniell window with a span of 20. Blue lines are the Markov red noise spectra. Dashed lines indicate upper and lower confidence bounds at 95% (red) and 90% (orange) significance levels.

however. The cause of such difference needs further investigation.

Differences in the interpretation of the major modes of Asian summer precipitation variability are noticed. Cook et al. (2010) discussed the major variability modes of the MADA using distinct EOF (DEOF) analysis. The MADA DEOF1 shows wet conditions over India and Southeast Asia (Fig. 3 in Cook et al. 2010), which was found associated with La Niña conditions. DEOF4 shows strong positive loading over the Tibetan Plateau, and it is associated with El Niño conditions. The MADA DEOF1 largely resembles the RAP EOF4, and the DEOF4 is likely corresponding to the RAP EOF1. However, the relative importance of these modes differs, with some fine spatial features in East Asia being less evident in the MADA than in the RAP. For example, the clear quadrupole pattern over East Asia depicted in the RAP EOF4 is very weak in the MADA DEOF1. In the MADA DEOF4, the wetting over the YRV during an El Niño condition might not be accurate (e.g., Yang et al. 2013a; Yang et al. 2014) in comparison with the unified drying over East China in the RAP EOF1. Li et al. (2014) showed similar MADA EOF

patterns as Cook et al. (2010), but both studies only discussed two modes of variability without discussing the periodicity of the PCs. In comparison with the MADA, the RAP provides a more comprehensive and perhaps more accurate description of the variability modes of the Asian summer precipitation in terms of a long reconstruction record.

Although the reconstruction made by Shi et al. (2017) is confined to China while the RAP covers all of Asia, they share very similar spatial patterns of the leading EOFs over China. Both reconstructions show a uniformed EOF1 pattern, a dipole EOF2 pattern, and a tripole EOF3 pattern (Fig. 8 in Shi et al. 2017). Shi et al. (2017) showed a significant connection between the Pacific decadal oscillation and the low-frequency PC2 (9-yr running average), which agrees with the RAP EOF2 as the interdecadal mode associated with mid-latitude northern Pacific Ocean SST variations. However, we do not think that this mode is associated with ENSO as suggested by Shi et al. (2017). Besides, the dynamical origins of the EOF1 and EOF3 of the RAP have been attributed to the biennial ENSO and CP El Niño–like decadal Pacific variability (Figs. 11 and 12), respectively, which are novel in the literature.
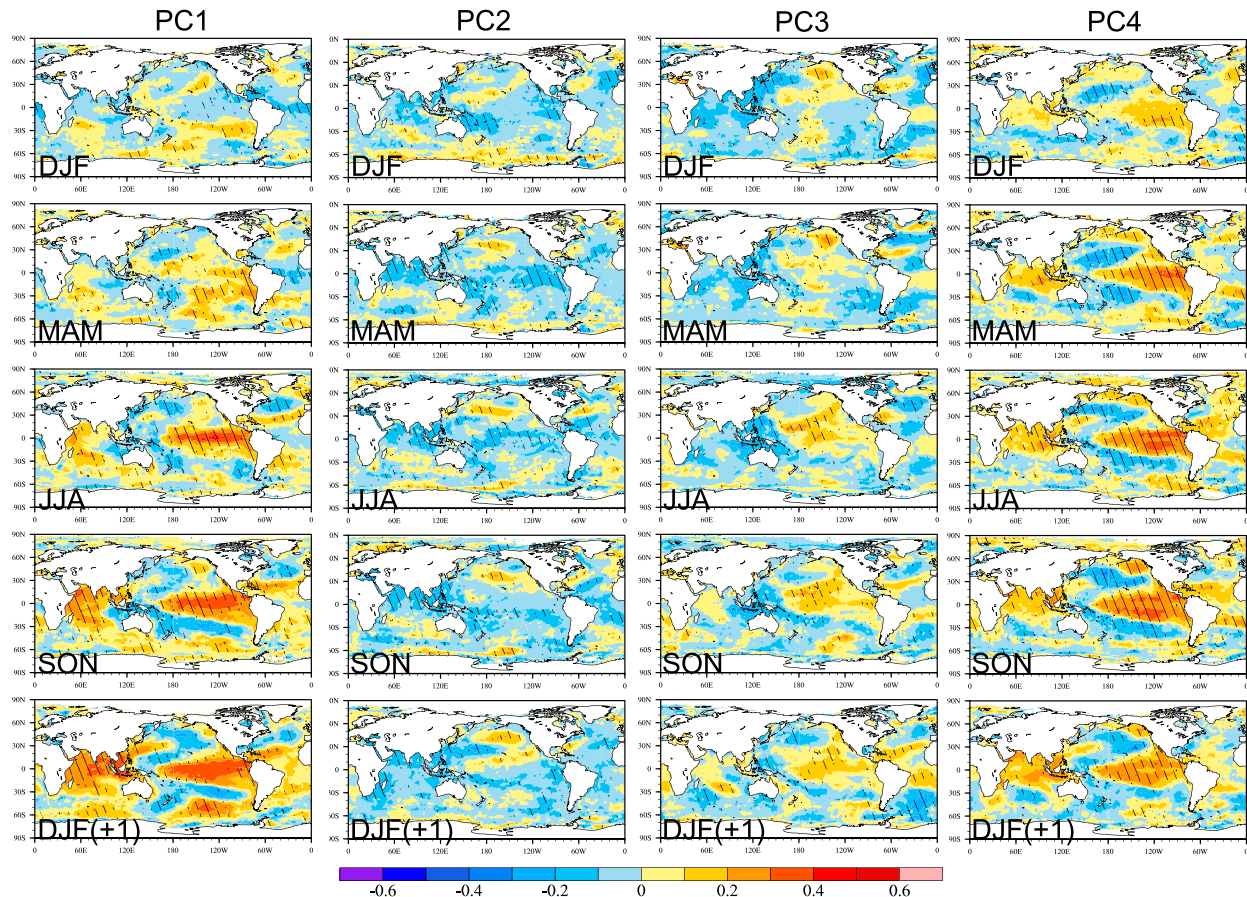
FIG. 12. Spatial patterns of correlations with global SSTs for each PC from 1871 to 2013. Each column represents correlations for one PC; seasonal evolutions of the PC–SST relations are shown from top to bottom. Hatched areas are significant correlations at 80% level and higher (2 tailed).

7. Conclusions

A 544-yr gridded (2° by 2°) summer (JJA) precipitation dataset was reconstructed for Asia (8.75°S–55.25°N, 61.25°–143.25°E) using complementary tree-ring chronologies and historical documentary records. The PPR method was used for reconstruction with the tree-ring width, and a frequency-based reconstruction method was applied to the historical documents. A new weighting method that was used to synthesize the two individual proxies yields quantitatively improved validation skill when compared with each individual reconstruction.

The quality and fidelity of the reconstructed Asian summer precipitation data have been extensively verified against the independent modern instrumental data over all of Asia (1901–20) and against the long-term rain gauge observations over India (1813–1920) and Seoul (1771–1920). The results show skillful reconstruction in East and North China, the Indochina Peninsula, the MC, northern India and Pakistan, midlatitude Asia, and southern Japan.

The RAP is best to illustrate large-scale rainfall variability, with more uncertainties in representing small-scale or local rainfall anomalies.

The RAP reproduces a realistic twentieth-century precipitation climatology. Four area-averaged precipitation indices were constructed for 1) all of Asia, 2) monsoon Asia, 3) arid (central and western) Asia, and 4) the MC. The interannual variations of the four indices show good agreement with observations during the twentieth century, indicating the ability of the RAP to capture large-scale year-to-year rainfall variability. For the preinstrumental period, general agreements are found between the RAP and other proxies such as the speleothem $\delta^{18}O$ record in China and India and ice cores over the Himalaya and the Tibetan Plateau on the decadal time scale. It also captures the remarkably abrupt change during the 1600s recorded in the upwelling proxy record over the Arabian Sea. While the results indicate that the RAP is to a certain degree reliable for long-term variability estimation, its accuracy is

limited by regional differences, observational coverage both in time and space, and precipitation regimes.

The 544-yr-long record of the RAP reveals four major modes of variability. The first EOF mode features unified drying over most parts of the AM system, and it is identified as forced by a rapidly developing El Niño or transition from a cold to a warm phase of the biennial ENSO mode. The second EOF is an interdecadal mode with wet conditions over the YRV and South China and dry conditions over India and northeastern Asia. The third EOF shows a tripole pattern over East Asia, and it is identified as related to a CP El Niño–like decadal mode in the Pacific. The fourth EOF features Indian and Southeast Asian dryness and a quadrupole pattern over East Asia. It is identified as associated with the low-frequency ENSO mode.

The results show that the RAP is able to describe long-term variability modes of Asian summer precipitation. It provides a valuable dataset for study of the large-scale Asian summer precipitation variability, especially on the decadal to centennial time scales, to aid our understanding of the attribution of these low-frequency processes.

REFERENCES

Anderson, D. M., J. T. Overpeck, and A. K. Gupta, 2002: Increase in the Asian southwest monsoon during the past four centuries. *Science*, **297**, 596–599, https://doi.org/10.1126/science.1072881.

Berkelhammer, M., A. Sinha, M. Mudelsee, H. Cheng, R. L. Edwards, and K. Cannariato, 2010: Persistent multidecadal power of the Indian summer monsoon. *Earth Planet. Sci. Lett.*, **290**, 166–172, https://doi.org/10.1016/j.epsl.2009.12.017.

Chen, J., and Coauthors, 2016: On the timing of the East Asian summer monsoon maximum during the Holocene—Does the speleothem oxygen isotope record reflect monsoon rainfall variability? *Sci. China Earth Sci.*, **59**, 2328–2338, https://doi.org/10.1007/s11430-015-5500-5.

Chen, Z., X. He, E. R. Cook, H.-S. He, W. Chen, Y. Sun, and M. Cui, 2011: Detecting dryness and wetness signals from tree-rings in Shenyang, northeast China. *Palaeogeogr. Palaeoclimatol. Palaeoecol.*, **302**, 301–310, https://doi.org/10.1016/j.palaeo.2011.01.018.

Cheng, H., and Coauthors, 2012: The climatic cyclicity in semiarid-arid central Asia over the past 500 000 years. *Geophys. Res. Lett.*, **39**, L01705, https://doi.org/10.1029/2011GL050202.

Chinese Academy of Meteorological Science China Meteorological Administration, 1981: *Yearly Charts of Dryness/Wetness in China for the Last 500-Year Period* (in Chinese). Cartological Press, 332 pp.

Clemens, S., 2006: Extending the historical record by proxy. *The Asian Monsoon*, B. Wang, Ed., Springer, 615–630.

Cook, E. R., 2015: Asian monsoon variability over the past millennium reconstructed from long tree-ring records: The Monsoon Asia Drought Atlas, version 2 (MADAv2). *AGU Chapman Conf. on Evolution of the Asian Monsoon and Its Impact on Landscape, Environment and Society: Using the Past as the Key to the Future*, Hong Kong, China, Amer. Geophys. Union, https://agu.confex.com/agu/monsoon/webprogram/Paper37251.html.

——, D. M. Meko, D. W. Stahle, and M. K. Cleaveland, 1999: Drought reconstructions for the continental United States. *J. Climate*, **12**, 1145–1163, https://doi.org/10.1175/1520-0442(1999)012<1145:DRFTCU>2.0.CO;2.

——, R. Seager, M. A. Cane, and D. W. Stahle, 2007: North American drought: Reconstructions, causes, and consequences. *Earth Sci. Rev.*, **81**, 93–134, https://doi.org/10.1016/j.earscirev.2006.12.002.

——, K. J. Anchukaitis, B. M. Buckley, R. D. D'Arrigo, G. C. Jacoby, and W. E. Wright, 2010: Asian monsoon failure and megadrought during the last millennium. *Science*, **328**, 486–489, https://doi.org/10.1126/science.1185188.

——, P. J. Krusic, K. J. Anchukaitis, B. M. Buckley, T. Nakatsuka, and M. Sano, 2013: Tree-ring reconstructed summer temperature anomalies for temperate East Asia since 800 C.E. *Climate Dyn.*, **41**, 2957–2972, https://doi.org/10.1007/s00382-012-1611-x.

Cosford, J., H. Qing, D. Mattey, B. Eglington, and M. Zhang, 2009: Climatic and local effects on stalagmite δ^{13}C values at Lianhua Cave, China. *Palaeogeogr. Palaeoclimatol. Palaeoecol.*, **280**, 235–244, https://doi.org/10.1016/j.palaeo.2009.05.020.

Dai, A., K. E. Trenberth, and T. Qian, 2004: A global dataset of Palmer Drought Severity Index for 1870–2002: Relationship with soil moisture and effects of surface warming. *J. Hydrometeor.*, **5**, 1117–1130, https://doi.org/10.1175/JHM-386.1.

DelSole, T., and J. Shukla, 2009: Artificial skill due to predictor screening. *J. Climate*, **22**, 331–345, https://doi.org/10.1175/2008JCLI2414.1.

Draper, N. R., and H. Smith, 1998: *Applied Regression Analysis*. John Wiley and Sons, 706 pp.

Duan, K., T. Yao, and L. G. Thompson, 2004: Low-frequency of southern Asian monsoon variability using a 295-year record from the Dasuopu ice core in the central Himalayas. *Geophys. Res. Lett.*, **31**, L16209, https://doi.org/10.1029/2004GL020015.

Fang, K., N. Davi, X. Gou, F. Chen, E. Cook, J. Li, and R. D'Arrigo, 2010: Spatial drought reconstructions for central

high Asia based on tree rings. *Climate Dyn.*, **35**, 941–951, https://doi.org/10.1007/s00382-009-0739-9.

Feng, S., Q. Hu, Q. Wu, and M. E. Mann, 2013: A gridded reconstruction of warm season precipitation for Asia spanning the past half millennium. *J. Climate*, **26**, 2192–2204, https://doi.org/10.1175/JCLI-D-12-00099.1.

Ge, Q., J. Zheng, Z. Hao, Y. Liu, and M. Li, 2016: Recent advances on reconstruction of climate and extreme events in China for the past 2000 years. *J. Geogr. Sci.*, **26**, 827–854, https://doi.org/10.1007/s11442-016-1301-4.

Goswami, B. N., M. S. Madhusoodanan, C. P. Neema, and D. Sengupta, 2006: A physical mechanism for North Atlantic SST influence on the Indian summer monsoon. *Geophys. Res. Lett.*, **33**, L02706, https://doi.org/10.1029/2005GL024803.

Gou, X., L. Gao, Y. Deng, F. Chen, M. Yang, and C. Still, 2015: An 850-year tree-ring-based reconstruction of drought history in the western Qilian Mountains of northwestern China. *Int. J. Climatol.*, **35**, 3308–3319, https://doi.org/10.1002/joc.4208.

Harris, I., P. D. Jones, T. J. Osborn, and D. H. Lister, 2014: Updated high-resolution grids of monthly climatic observations—the CRU TS3.10 dataset. *Int. J. Climatol.*, **34**, 623–642, https://doi.org/10.1002/joc.3711.

Kang, S., A. Bräuning, and H. Ge, 2014: Tree-ring based evidence of the multi-decadal climatic oscillation during the past 200 years in north-central China. *J. Arid Environ.*, **110**, 53–59, https://doi.org/10.1016/j.jaridenv.2014.06.003.

Li, H., D. Gu, T. Ku, L. D. Stott, and W. Chen, 1998: Applications of interannual-resolution stable isotope records of speleothem: Climatic changes in Beijing and Tianjin, China during the past 500 years—the δ^{18}O record. *Sci. China*, **41D**, 362–368, https://doi.org/10.1007/BF02932686.

Li, J., X. Gou, E. R. Cook, and F. Chen, 2006: Tree-ring based drought reconstruction for the central Tien Shan area in northwest China. *Geophys. Res. Lett.*, **33**, L07715, https://doi.org/10.1029/2006GL025803.

——, S.-P. Xie, and E. R. Cook, 2014: El Niño phases embedded in Asian and North American drought reconstructions. *Quat. Sci. Rev.*, **85**, 20–34, https://doi.org/10.1016/j.quascirev.2013.11.014.

Li, Z. H., J. H. Zhu, J. N. Cai, and S. W. Wang, 2005: Flood in Huaihe valley since 1470 (in Chinese). *Meteorology*, **31**, 24–28.

Rayner, N. A., D. E. Parker, E. B. Horton, C. K. Folland, L. V. Alexander, D. P. Rowell, E. C. Kent, and A. Kaplan, 2003: Global analyses of sea surface temperature, sea ice, and night marine air temperature since the late nineteenth century. *J. Geophys. Res.*, **108**, 4407, https://doi.org/10.1029/2002JD002670.

Schneider, U., A. Becker, P. Finger, A. Meyer-Christoffer, B. Rudolf, and M. Ziese, 2015: GPCC full data reanalysis at 0.5°: Monthly land-surface precipitation from rain-gauges built on GTS-based and historic data, version 7.0. Global Precipitation and Climatology Centre, accessed 7 November 2017, https://doi.org/10.5676/DWD_GPCC/FD_M_V7_050.

Shao, X., L. Huang, H. Liu, E. Liang, X. Fang, and L. Wang, 2005: Reconstruction of precipitation variation from tree rings in recent 1000 years in Delingha, Qinghai. *Sci. China*, **48D**, 939–949, https://doi.org/10.1360/03yd0146.

Shi, F., B. Yang, A. Mairesse, L. Von Gunten, J. Li, A. Bräuning, F. Yang, and X. Xiao, 2013: Northern Hemisphere temperature reconstruction during the last millennium using multiple annual proxies. *Climate Res.*, **56**, 231–244, https://doi.org/10.3354/cr01156.

——, J. Li, and R. J. S. Wilson, 2014: A tree-ring reconstruction of the South Asian summer monsoon index over the past millennium. *Sci. Rep.*, **4**, 6739, https://doi.org/10.1038/srep06739.

——, S. Zhao, Z. Guo, H. Goosse, and Q. Yin, 2017: Multi-proxy reconstructions of May–September precipitation field in China over the past 500 years. *Climate Past*, **13**, 1919–1938, https://doi.org/10.5194/cp-13-1919-2017.

Sinha, A., M. Berkelhammer, L. Stott, M. Mudelsee, H. Cheng, and J. Biswas, 2011: The leading mode of Indian summer monsoon precipitation variability during the last millennium. *Geophys. Res. Lett.*, **38**, L15703, https://doi.org/10.1029/2011GL047713.

——, G. Kathayat, H. Cheng, S. F. M. Breitenbach, M. Berkelhammer, M. Mudelsee, J. Biswas, and R. L. Edwards, 2015: Trends and oscillations in the Indian summer monsoon rainfall over the last two millennia. *Nat. Commun.*, **6**, 6309, https://doi.org/10.1038/ncomms7309.

Sontakke, N. A., N. Singh, and H. N. Singh, 2008: Instrumental period rainfall series of the Indian region (AD 1813–2005): Revised reconstruction, update and analysis. *Holocene*, **18**, 1055–1066, https://doi.org/10.1177/0959683608095576.

Tan, L., Y. Cai, H. Cheng, Z. An, and R. L. Edwards, 2009: Summer monsoon precipitation variations in central China over the past 750 years derived from a high-resolution absolute-dated stalagmite. *Palaeogeogr. Palaeoclimatol. Palaeoecol.*, **280**, 432–439, https://doi.org/10.1016/j.palaeo.2009.06.030.

——, ——, Z. An, R. L. Edwards, H. Cheng, C.-C. Shen, and H. Zhang, 2011: Centennial- to decadal-scale monsoon precipitation variability in the semi-humid region, northern China during the last 1860 years: Records from stalagmites in Huangye Cave. *Holocene*, **21**, 287–296, https://doi.org/10.1177/0959683610378880.

——, and Coauthors, 2015: A Chinese cave links climate change, social impacts, and human adaptation over the last 500 years. *Sci. Rep.*, **5**, 12284, https://doi.org/10.1038/srep12284.

Tan, M., 2016: Circulation background of climate patterns in the past millennium: Uncertainty analysis and re-reconstruction of ENSO-like state. *Sci. China Earth Sci.*, **59**, 1225–1241, https://doi.org/10.1007/s11430-015-5256-6.

Thompson, L. G., and Coauthors, 1997: Tropical climate instability: The last glacial cycle from a Qinghai-Tibetan ice core. *Science*, **276**, 1821–1825, https://doi.org/10.1126/science.276.5320.1821.

——, T. Yao, E. Mosley-Thompson, M. E. Davis, K. A. Henderson, and P.-N. Lin, 2000: A high-resolution millennial record of the South Asian monsoon from Himalayan ice cores. *Science*, **289**, 1916–1919, https://doi.org/10.1126/science.289.5486.1916.

——, and Coauthors, 2006a: Abrupt tropical climate change: Past and present. *Proc. Natl. Acad. Sci. USA*, **103**, 10 536–10 543, https://doi.org/10.1073/pnas.0603900103.

——, T. Yao, M. E. Davis, E. Mosley-Thompson, T. A. Mashiotta, P.-N. Lin, V. N. Mikhalenko, and V. S. Zagorodnov, 2006b: Holocene climate variability archived in the Puruogangri ice cap on the central Tibetan Plateau. *Ann. Glaciol.*, **43**, 61–69, https://doi.org/10.3189/172756406781812357.

Wang, B., and Q. Ding, 2008: Global monsoon: Dominant mode of annual variation in the tropics. *Dyn. Atmos. Oceans*, **44**, 165–183, https://doi.org/10.1016/j.dynatmoce.2007.05.002.

——, ——, and J.-G. Jhun, 2006: Trends in Seoul (1778–2004) summer precipitation. *Geophys. Res. Lett.*, **33**, L15803, https://doi.org/10.1029/2006GL026418.

——, and Coauthors, 2009: Advance and prospectus of seasonal prediction: Assessment of the APCC/CliPAS 14-model ensemble retrospective seasonal prediction (1980–2004). *Climate Dyn.*, **33**, 93–117, https://doi.org/10.1007/s00382-008-0460-0.

——, and Coauthors, 2018: Toward predicting changes in the land monsoon rainfall a decade in advance. *J. Climate*, **31**, 2699–2714, https://doi.org/10.1175/JCLI-D-17-0521.1.

Wang, P., S. Clemens, L. Beaufort, P. Braconnot, G. Ganssen, Z. Jian, P. Kershaw, and M. Sarnthein, 2005: Evolution and variability of the Asian monsoon system: State of the art and outstanding issues. *Quat. Sci. Rev.*, **24**, 595–629, https://doi.org/10.1016/j.quascirev.2004.10.002.

——, B. Wang, H. Cheng, J. Fasullo, Z. T. Guo, T. Kiefer, and Z. Y. Liu, 2014: The global monsoon across timescales: Coherent variability of regional monsoons. *Climate Past*, **10**, 2007–2052, https://doi.org/10.5194/cp-10-2007-2014.

Wang, S., and Z. C. Zhao, 1979: An analyses of historical data of droughts and floods in last 500 years in China (in Chinese). *Acta Geogr. Sin.*, **34**, 329–342, https://doi.org/10.11821/xb197904005.

——, D. Y. Gong, J. L. Ye, and Z. H. Chen, 2000: Seasonal precipitation series of eastern China since 1880 and the variability. *Acta Geogr. Sin.*, **67**, 281–293, https://doi.org/10.11821/xb200003004.

Wang, Y., and Coauthors, 2005: The Holocene Asian monsoon: Links to solar changes and North Atlantic climate. *Science*, **308**, 854–857, https://doi.org/10.1126/science.1106296.

Webster, P. J., 2006: The coupled monsoon system. *The Asian Monsoon*, B. Wang, Ed., Springer, 3–66.

——, V. O. Magaña, T. N. Palmer, J. Shukla, R. A. Tomas, M. Yanai, and T. Yasunari, 1998: Monsoons: Processes, predictability, and the prospects for prediction. *J. Geophys. Res.*, **103**, 14 451–14 510, https://doi.org/10.1029/97JC02719.

Xu, C., M. Sano, and T. Nakatsuka, 2013: A 400-year record of hydroclimate variability and local ENSO history in northern Southeast Asia inferred from tree-ring δ^{18}O. *Palaeogeogr. Palaeoclimatol. Palaeoecol.*, **386**, 588–598, https://doi.org/10.1016/j.palaeo.2013.06.025.

Xu, H., and Coauthors, 2015: Late Holocene Indian summer monsoon variations recorded at Lake Erhai, southwestern China. *Quat. Res.*, **83**, 307–314, https://doi.org/10.1016/j.yqres.2014.12.004.

Yang, B., S. Kang, F. C. Ljungqvist, M. He, Y. Zhao, and C. Qin, 2014: Drought variability at the northern fringe of the Asian summer monsoon region over the past millennia. *Climate Dyn.*, **43**, 845–859, https://doi.org/10.1007/s00382-013-1962-y.

Yang, F., F. Shi, S. Kang, S. Wang, Z. Xiao, T. Nakatsuka, and J. Shi, 2013a: Comparison of the dryness/wetness index in China with the Monsoon Asia Drought Atlas. *Theor. Appl. Climatol.*, **114**, 553–566, https://doi.org/10.1007/s00704-013-0858-4.

——, N. Wang, F. Shi, F. C. Ljungqvist, S. Wang, Z. Fan, and J. Lu, 2013b: Multi-proxy temperature reconstruction from the west Qinling Mountains, China, for the past 500 years. *PLOS ONE*, **8**, e57638, https://doi.org/10.1371/journal.pone.0057638.

Yi, L., H. Yu, J. Ge, Z. Lai, X. Xu, L. Qin, and S. Peng, 2012: Reconstructions of annual summer precipitation and temperature in north-central China since 1470 AD based on drought/flood index and tree-ring records. *Climatic Change*, **110**, 469–498, https://doi.org/10.1007/s10584-011-0052-6.

Zhang, D., 1983: Method to reconstruct climatic series for the past 500 years and its reliability. *Collect. Pap. Meteor. Sci. Technol.*, **4**, 17–26.

——, and C. Liu, 1993: Continuation (1980–1992) of the yearly charts of dryness/wetness in China for the last 500 years period. *Meteor. Mon.*, **19**, 41–45.

Zhang, P., and Coauthors, 2008: A test of climate, sun, and culture relationships from an 1810-year Chinese cave record. *Science*, **322**, 940–942, https://doi.org/10.1126/science.1163965.

Zhang, Q.-B., G. Cheng, T. Yao, X. Kang, and J. Huang, 2003: A 2,326-year tree-ring record of climate variability on the northeastern Qinghai-Tibetan Plateau. *Geophys. Res. Lett.*, **30**, 1739, https://doi.org/10.1029/2003GL017425.

Zheng, J., Q. Ge, Z. Hao, H. Liu, Z. Man, Y. Hou, and X. Fang, 2014a: Paleoclimatology proxy recorded in historical documents and method for reconstruction on climate change (in Chinese). *Quat. Sci.*, **34**, 1186–1196.

——, Z. Hao, X. Fang, and Q. Ge, 2014b: Changing characteristics of extreme climate events during past 2000 years in China. *Prog. Geogr.*, **33**, 3–12, https://doi.org/10.11820/dlkxjz.2014.01.001.

Zhu, J., and S. Wang, 2002: 80 yr oscillation of summer rainfall over North China and East Asian summer monsoon. *Geophys. Res. Lett.*, **29**, 1672, https://doi.org/10.1029/2001GL013997.